IEEE Access
Multidisciplinary ⋮ Rapid Review ⋮ Open Access Journal

Received October 12, 2020, accepted October 26, 2020, date of publication October 29, 2020, date of current version November 10, 2020.

Digital Object Identifier 10.1109/ACCESS.2020.3034667

Influence of Introducing the Rotor MMF Harmonic on Torque Performance of Spoke Type Permanent Magnet Motor With FSCW

JIAXU ZHANG, BINGYI ZHANG, AND GUIHONG FENG
School of Electrical Engineering, Shenyang University of Technology, Shenyang 110870, China
Corresponding author: Guihong Feng (78908410@qq.com)

ABSTRACT This article proposes a torque optimization method that introduces the rotor magnetomotive force (MMF) harmonics, aiming to increase the average torque without increasing the cogging torque and torque ripple. A spoke type permanent magnet direct drive motor with fractional slot concentrated winding (FSCW) is designed. The FSCW can improve the utilization rate of the winding, but at the same time, it brings a wealth of MMF harmonics. First, the electromagnetic torque expression is derived using the principles of magnetic energy and virtual power. It means that the constant electromagnetic torque is generated when the stator and rotor MMF harmonics with the same space and time order are the same as the main wave speed. The analytical method is then used to analyze the influence of the stator and rotor MMF harmonics on the electromagnetic torque of the three-phase FSCW permanent magnet motor. On this basis, a rotor shape that introduces the third rotor MMF harmonics is proposed. Finally, the finite element software is used to compare and analyze the torque performance of motor before and after optimization. The finite element simulation and experiment results prove the correctness and effectiveness of the method.

INDEX TERMS Spoke type permanent magnet direct drive motor, fractional slot concentrated winding, MMF harmonics, torque optimization.

I. INTRODUCTION

The fractional slot concentrated winding (FSCW) permanent magnet motors have become a hot spot in domestic and foreign research due to their high torque density, simple winding structure, small cogging torque, and high efficiency. They are widely used in direct drive systems such as CNC machine tool turntables, aerospace, mining machinery, and robot elbow joints [1]–[3]. The spoke type permanent magnet (PM) motor has a significant magnetizing effect compared with the radial structure, so it is widely used in occasions requiring high torque density; at the same time, compared with the radial structure, the spoke type structure could place more permanent magnets in the circumferential direction, so the number of poles of the spoke type motor could be designed more. The motor can be designed for lower speed [4]. Optimizing rotor pole shape can effectively reduce partial demagnetization effect and cogging torque in spoke type brushless PM motor [5].

Mining belt conveyor drive motor adopts FSCW spoke type permanent magnet direct drive motor, which can realize low-speed and high-torque operation, directly drive the load, minimize the transmission link, and improve the reliability and efficiency of the drive system. However, the direct-drive system of the belt conveyor cancels the mechanical transmission structure, such as the reducer, which requires the motor to have the characteristics of high torque density and low speed. In addition, FSCW can improve winding utilization and reduce the copper volume and copper loss at the end of the stator winding. At the same time, it will also bring rich MMF harmonics [6]–[8], which will affect the torque performance of the motor. Therefore, it is necessary to study the magnetic harmonic content and distribution characteristics in detail. A closed-form analytical model is proposed in [9], which can analyze surface PM machines designed with FSCW. Special features of the FSCWs are taken into account, including stator slot effects.

The direct-drive, low-speed operation, high torque density, and low torque ripple is urgently needed for the belt conveyor drive system. Although employing high-grade rare earth PM materials is one way to improve the torque density of permanent magnet synchronous motors (PMSMs), other design methodologies can further improve the torque performance. For surface permanent magnet motor (SPM), the air-gap

The associate editor coordinating the review of this manuscript and approving it for publication was Zhong Wu.

permeance is almost constant due to the relative permeability of PMs almost equal to unity and hence the sinusoidal air-gap flux density can be achieved by shaping PMs to achieve low torque ripple [10]–[12], but the torque density is usually considerably compromised. In [13], a novel shaped-magnet surface permanent magnet machine design concept featuring magnets shaped is proposed according to a sinusoid plus a third harmonic along the axial direction for high-performance motor applications that require high torque density and minimal torque ripple. However, the shape of the permanent magnet is more complex. It is worth noting that the optimal cogging torque is not necessarily the optimal design of the minimum torque ripple [14], [15]. In [14], a simple solution for minimizing the cogging torque and suppressing operation torque ripple simultaneously is presented. The principle of that simple solution is illustrated, where a magnet with different width is used so that the flux density distribution in the machine is substantially changed. In [15], taking the slot opening design as an example, the design tradeoff between the open-circuit cogging torque and the on-load torque ripple is investigated. In [16], [17], a low-speed and high-torque permanent magnet motor with a dual-stator structure is proposed to increase the torque density of the motor. However, the disadvantage is that the structure is complex, and the process requirements are high. Of course, many current references were also forced on improving the torque performance by multi-objective optimization strategy, not only in the field of a structure optimization but also in the control strategy. Reference [18] proposed a regenerative braking control strategy based on multi-objective optimization of switched reluctance generator (SRG) drive system, which increases the vehicle braking comfort and improves battery lifetime without decreasing recovery energy. Three optimization indexes were considered in the paper: power generation, torque ripple, and current fluctuation. Reference [19] developed a geometrical multi-objective optimization strategy to improve the static torque performance of the SRM with two-phase mode. Therefore, the multi-objective optimization strategy can be targeted and better to improve the performance of the motor. The primary purpose of this article is to study the influence of rotor MMF and harmonics on the torque performance of the motor. Therefore, only the rotor shape factor that introduces the rotor MMF harmonics is considered, and the optimization design of other geometric structure parameters is not considered. For the low-speed high-torque spoke type PM motor proposed in this article, the torque performance of the motor is optimized by optimizing the shape of the rotor sheet. The cogging torque and torque ripple are reduced without changing the shape of the PM. Besides, compared with the anisotropic PM, the rectangular PM is easy to process and reduces the cost.

This article proposes a torque optimization method for the shape of the rotor that introduces the third harmonic of the rotor magnetomotive force (MMF) and designs a spoke type permanent magnet motor, which aims to improve the average torque without increasing cogging torque and torque ripple. This article will be organized as follows. Section II uses the MMF method and the principle of virtual power to analyze the principle of electromagnetic torque generation of the motor and gives the conditions for generating constant electromagnetic torque and pulsating electromagnetic torque. Section III uses the analytical method and the finite element method to analyze the armature MMF of the FSCW motor. In Section IV, the stator and rotor MMF harmonics of a three-phase FSCW permanent magnet motor and their influence on torque performance are studied. In Section V, based on the above analysis, a prototype was designed using the torque optimization method proposed. The electromagnetic field finite element analysis (FEA) of the motor before and after optimization is carried out, and the average torque, cogging torque, and torque ripple are compared. The simulation results are consistent with the theoretical analysis and finally verified by experiments.

II. THE RELATIONSHIP BETWEEN ELECTROMAGNETIC TORQUE AND MMF

Assuming that the magnetic permeability of the motor core is infinite, that is, all the magnetic field energy is stored in the air-gap, and the stator MMF is ahead of the rotor MMF δ_{vn} (electrical angle), considering time harmonics and space harmonics, the expression of the magnetic field generated by the stator and rotor magnetomotive force in the air-gap can be written as follows:

$$B_s = \frac{\mu_0}{g}\sum_{\mu}\sum_{v} F_{s\mu v}\cos(\mu\omega t - v\theta_s) \tag{1}$$

$$B_r = \frac{\mu_0}{g}\sum_{m}\sum_{n} F_{rmn}\cos(m\omega t - n\theta_s - \delta_{vn}) \tag{2}$$

where μ_0 is the vacuum permeability, ω is the stator angular frequency, μ and v is the stator MMF time harmonic order and space harmonic order respectively, m and n is the rotor MMF time harmonic order and space harmonic order respectively, θ_s is the angle between the rotor pole axis and phase A winding axis along the air-gap circumference, $F_{s\mu v}$ and F_{rmn} is the stator and rotor MMF amplitude respectively; g is the equivalent air-gap length.

Eq. (1) and (2) include all the time and space harmonics of stator and rotor.

The magnetic field energy stored in the air-gap is:

$$W_m = \int_V \frac{B^2}{2\mu_0}\mathrm{d}V = \frac{gl}{4\mu_0}\frac{D}{p}\int_0^{2p\pi}(B_s + B_r)^2\mathrm{d}\theta_s \tag{3}$$

where l is the length of the stator core, p is the pole pairs, D is the average diameter of the air-gap, V is the unit air-gap volume.

Incorporating Eq. (1) and (2) into Eq. (3), and then using the orthogonality of the trigonometric function, the simplified formula can be obtained as follows:

$$W_m = \frac{\mu_0 l\pi D}{4g}[\sum_{\mu}\sum_{v}F_{s\mu v}^2 + \sum_{m}\sum_{n}F_{rmn}^2 + \sum_{v\neq n}0 + 2\sum_{v=n}\sum_{\mu}\sum_{m}F_{s\mu v}F_{rmn}\cos(\mu\omega t - m\omega t + \delta_{vn})] \tag{4}$$

The electromagnetic torque under the action of the stator and rotor magnetic field can be obtained by calculating the partial derivative of the rotor position in the above Equation while keeping the amplitude of MMF unchanged. Assuming the differential virtual displacement of the rotor $\Delta\delta_{vn}$, the electromagnetic torque can be obtained from Eq. (4):

$$T_e = p\frac{\partial W_m}{\partial\,\delta_{vn}} = \sum_{v\neq n} 0 - p\frac{\mu_0 l\pi D}{2g} \cdot \sum_{v=n}\sum_{\mu}\sum_{m} F_{s\mu v}\,F_{rmn}\cos(\mu\omega t - m\omega\, t + \delta_{vn}) \tag{5}$$

From Eq. (5), the following conclusions can be obtained:

(1) The stator MMF and the rotor MMF harmonics have the same space order ($v = n$), they interact to produce electromagnetic torque. If the space order is different ($v \neq n$), the interaction between them does not produce electromagnetic torque. If the stator MMF and the rotor MMF harmonics have the same space order ($v = n$) and different time order ($\mu \neq m$), then the interaction between them only produces pulsating electromagnetic torque.

(2) Only when the stator and rotor MMF harmonics with the same time order ($v = n$) and space order ($\mu = m$) interact, it is possible to produce a constant electromagnetic torque. When the maximum constant electromagnetic torque is generated, the time and space MMF harmonics are defined as the main wave, and the speed is ω, then the MMF harmonics with the same speed as the main wave can produce constant electromagnetic torque, while the MMF harmonics inconsistent with the main wave speed can only produce pulsating torque.

III. ANALYSIS OF ARMATURE MMF OF FSCW

A. FRACTIONAL SLOT CONCENTRATED WINDING MOTOR

For FSCWs, the number of slots per pole per phase q can be expressed as follows:

$$q = \frac{Z}{2m_1 p} = \frac{N}{d} \tag{6}$$

where N/d is the irreducible true fraction, m_1 is the number of phases, Z is the number of stator slots, and p is the pole pairs. When d is an even number, the main wave is $d/2$; when d is an odd number, the main wave is d. If each harmonic is divided by order of the main wave, the order of the main wave will become 1, which is the fundamental wave. The other harmonics are the fractional harmonic and higher-order harmonic in fractional slot winding motor [20].

In general, there is a greatest common divisor t between the slots Z and pole pairs p of FSCW motor, that is:

$$t = \frac{Z}{p} = \gcd(Z, p) \tag{7}$$

If $Z_0 = Z/t$, $p_0 = p/t$, then q can be rewritten as follows:

$$q = \frac{Z_0}{2m_1 p_0} \tag{8}$$

Therefore, the motor with slots Z_0 and pole pairs p_0 is called a unit motor, and the original motor consists of t unit motors.

B. HARMONIC ANALYSIS OF STATOR MMF OF 10-POLE 12-SLOT MOTOR

The prototype designed in this article is a three-phase 40-pole 48-slot permanent magnet direct-drive motor. The winding form is a double layer Y-type connection and a spoke type structure. As shown in Fig. 1, the shaft and the magnetic insulation are connected by a support plate, which can reduce the amount of rotor lamination and reduce the cost, and the rotor and the magnetic insulation are fixed by bolts. The original motor consists of four 10-pole 12-slot unit motors. Therefore, this section takes a 10-pole 12-slot unit motor as an example for analysis.

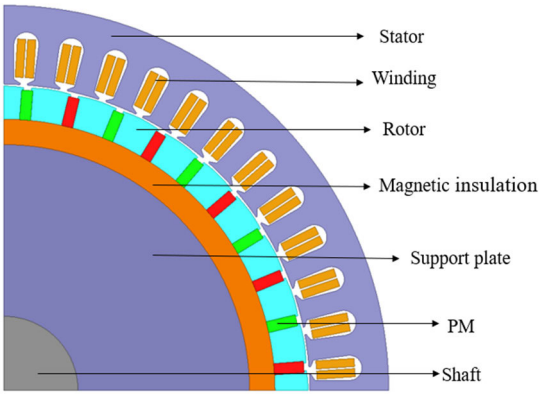

FIGURE 1. The structure model of the proposed motor.

To facilitate the analysis, make the following assumptions:

(1) The magnetic circuit of the motor is not saturated;

(2) The stator and rotor permeance of the motor is infinite;

(3) Ignore the cogging effect.

For a unit motor with a stator slot number Z_0, rotor pole pairs number p_0, and coil turns number N_0, when the maximum instantaneous value I of sinusoidal alternating current flows through the coil, the MMF waveform generated by the coil is a rectangular wave with different positive and negative amplitudes but equal positive and negative areas. Take the MMF waveform generated by a coil with a span of $y = 1$ as an example, as shown in Fig. 2.

where:

$$S_1 = S_2 + S_3 \tag{9}$$

$$S_2 = S_3 \tag{10}$$

$$\mathrm{F}_+ = IN_0(Z_0 - 1)/Z_0 \tag{11}$$

$$\mathrm{F}_- = IN_0/Z_0 \tag{12}$$

To obtain the MMF waveform of each phase winding, the connection mode of stator winding should be determined firstly, and then the three-phase MMF waveform can be obtained by superposition of MMF of each phase winding. Fig. 3 shows the expansion diagram of the stator winding connection of the 10-pole 12-slot unit motor. Assuming that the

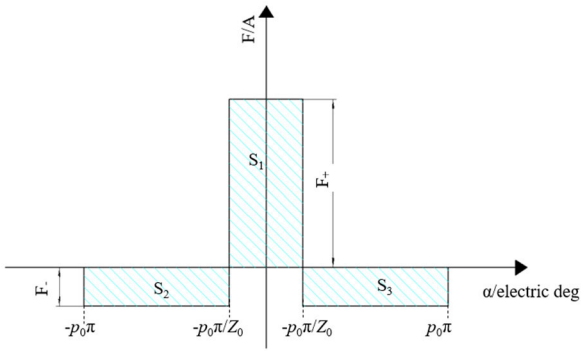

FIGURE 2. MMF waveform generated by one coil.

instantaneous maximum value of phase current is $i_a = I$, then the current of phase B and phase C is $i_b = i_c = -I/2$. The MMF waveform at this moment is shown in Fig. 4. Among them, Fig. 4 (a) is the MMF waveform comparison between the analytical method and the finite element method (FEM), and Fig. 4 (b) is the FFT analysis of the MMF waveform obtained by FEM. It can be seen that the results obtained by the two methods are basically consistent, but the MMF waveform obtained by the FEM has troughs in the rotor position mechanical angle of 105 deg and 285 deg. This is because the cogging effect is not ignored in the FEM calculation. The paper takes 10-pole 12-slots as an example, the winding span is 1, and the tooth pitch is 30 deg (mech.deg). Therefore, the stator MMF waveform will have a trough in a tooth pitch. The three-phase composite stator MMF has the same phase in the range of 75 deg - 135 deg and 255 deg - 315 deg, while the phase of stator MMF in other adjacent tooth regions is opposite. Therefore, the stator MMF waveform obtained by the FEM has wave troughs at 105 deg and 285 deg. The MMF harmonics generated by the FSCW are very rich, but only the 5th harmonic interacts with the permanent magnet magnetic field to produce a constant electromagnetic torque, and there is no third stator MMF. The potential harmonics will be analyzed in detail later.

IV. INFLUENCE OF STATOR AND ROTOR MMF HARMONICS ON TORQUE OF THREE-PHASE FSCW MOTOR

A. THREE-PHASE WINDING COMPOSITE MMF INCLUDING SPACE-TIME HARMONICS

Assume that the stator current contains harmonics of 1, 3, 5, 7, 9, 11, 13, etc., the expression of stator current is as follows:

$$\begin{cases} i_a(t) = \sum\limits_{\mu=1,3,5,\cdots}^{\infty} I_{\varphi\mu} \cos \mu\omega t \\ i_b(t) = \sum\limits_{\mu=1,3,5,\cdots}^{\infty} I_{\varphi\mu} \cos \mu(\omega t - 120^\circ) \\ i_c(t) = \sum\limits_{\mu=1,3,5,\cdots}^{\infty} I_{\varphi\mu} \cos \mu(\omega t - 240^\circ) \end{cases} \tag{13}$$

where $I_{\varphi\mu}$ is the amplitude of harmonic current.

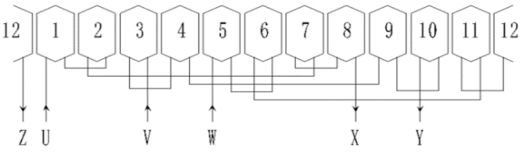

FIGURE 3. Winding development of 10-pole 12-slot unit motor.

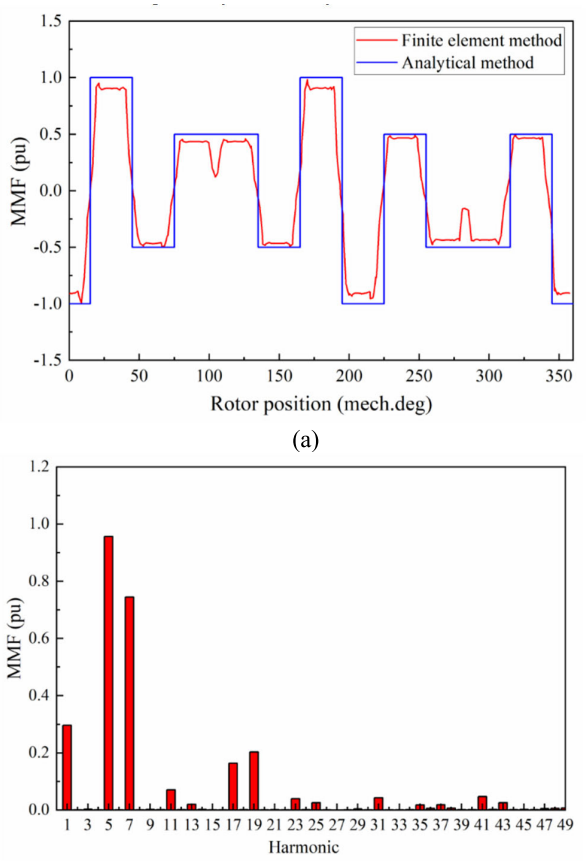

FIGURE 4. The MMF distribution of 12-slot 10-pole unit motor. (a) MMF waveform comparison between analytical method and FEM (b) Harmonic analysis of MMF obtained by FEM.

With the axis of phase A winding as the spatial reference axis, it is assumed that at a certain time, at a distance θ_s from the axis of phase A winding, the MMF of each phase winding is:

$$\begin{cases} f_a(t) = \sum\limits_{\mu=1,3,5\cdots}^{\infty} \sum\limits_{\nu=1,3,5\cdots}^{\infty} F_{\varphi\nu} I_{\varphi\mu} \cos \nu\theta_s \cos \mu\omega t \\ f_b(t) = \sum\limits_{\mu=1,3,5\cdots}^{\infty} \sum\limits_{\nu=1,3,5\cdots}^{\infty} F_{\varphi\nu} I_{\varphi\mu} \cos \nu(\theta_s - 120^\circ) \\ \qquad \times \cos \mu(\omega t - 120^\circ) \\ f_c(t) = \sum\limits_{\mu=1,3,5\cdots}^{\infty} \sum\limits_{\nu=1,3,5\cdots}^{\infty} F_{\varphi\nu} I_{\varphi\mu} \cos \nu(\theta_s - 240^\circ) \\ \qquad \times \cos \mu(\omega t - 240^\circ) \end{cases} \tag{14}$$

Adding the three-phase pulsating MMF in Eq. (14), the composite stator MMF of different time and space times can be obtained:

$$\begin{aligned} f_s &= f_a(t) + f_b(t) + f_c(t) \\ &= \frac{3}{2} \sum_{\mu=\nu=1,5,7\cdots}^{\infty} F_{\varphi\nu} I_{\varphi\mu} \cos(\nu\theta_s - \mu\omega t) \\ &\quad \pm \frac{3}{2} \sum_{\substack{\mu=\nu=\pm 6k, \\ \mu\neq 3i, \nu\neq 3j}}^{\infty} F_{\varphi\nu} I_{\varphi\mu} \cos(\nu\theta_s \pm \mu\omega t) \\ &\quad + \frac{3}{2} \sum_{\mu=3i}^{\infty} \sum_{\nu=3j}^{\infty} F_{\varphi\nu} I_{\varphi\mu} \left[\cos(\nu\theta_s + \mu\omega t) + \cos(\nu\theta_s - \mu\omega t)\right] \\ &\quad (k, i, j = 1, 2, 3\cdots) \end{aligned} \tag{15}$$

The following conclusions can be obtained from Eq. (15):

(1) When $\mu = \nu = 1, 5, 7, 11, 13, 17\cdots$, the composite MMF is positive rotation and the rotational speed is ω;

(2) When $\mu - \nu = \pm 6k$, $\mu \neq 3i, \nu \neq 3j, (i, j, k = 1, 2, 3\cdots)$, when ν takes a positive value, the composite MMF rotates forward. When ν takes a negative value, the resultant MMF rotates in the reverse direction, and the speed is $\mu\omega/\nu$. If it is inconsistent with the main wave speed, ripple torque will be generated, that is the ripple torque of 6th, 12th, 18th, etc. in the three-phase motor;

(3) When $\mu = 3i$ and $\nu = 3j(i, j = 1, 3, 5, 7\cdots)$, the composite MMF is pulsating;

(4) For the sum of other groups of μ and ν, the composite MMF is zero.

In this article, the space-time MMF harmonics are expressed as (μ, ν), if the order of the main wave is (1, 1), then when the time harmonic $\mu = 1$, the rotational speed of the (1, 5) MMF harmonic is 1/5 of the main wave, and the rotation of them is opposite, resulting in the 6th ripple torque; while the rotation speed of the (1, 7) MMF harmonic is 1/7 of the main wave, but the rotation of them is the same, so they also produce the 6th ripple torque; similarly, the (5, 1) and (5, 11) MMF harmonics produce the 6th ripple torque. The speed and direction of (5, 5) MMF harmonics are the same as that of the main wave, resulting in constant electromagnetic torque. The analysis of the influence of other harmonics on the torque is the same.

B. THE MMF OF ROTOR

The rotor MMF of the spoke type permanent magnet motor is provided by permanent magnets. The PM provides the cross-sectional area of the magnetic flux per pole is $A_{\mathrm{m}} = 2b_m l_m$, which is twice that of the radial magnetic pole structure. b_m and l_m are the width and axial length of the PM respectively. Besides, the d-axis and q-axis are also different from the radial structure. For the spoke type pole structure, the d-axis is located at the centerline of the rotor sheet, and the q-axis is located at the centerline of the PM, as shown in Fig. 5.

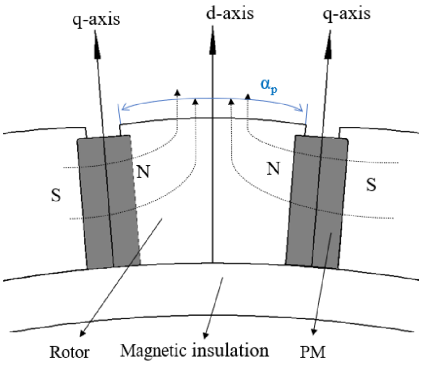

FIGURE 5. Spoke type rotor structure.

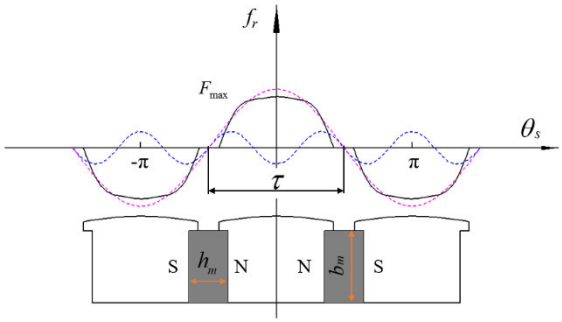

FIGURE 6. Magnetic field distribution of rotor MMF.

The radial air-gap flux density waveform generated by the rotor excitation magnetic field in the air-gap is related to the size of the PM, the magnetization method, and the external magnetic circuit. The influence of slotting and magnetic leakage is ignored. Taking the PM motor with a uniform air-gap and parallel magnetization as an example for analysis, it can be considered that the magnetic field generated in the air-gap is a trapezoidal wave, as shown in Fig. 6, where b_m is the width of the PM, τ is the pole pitch, h_m is is the thickness of the PM in the magnetizing direction and $F_{\max}$ is the rotor MMF amplitude. Assuming that the rotor speed is the same as the main wave speed, the Fourier series expression of the rotor MMF is:

$$f_r = \sum_{n=1,3,5\cdots}^{\infty} F_{\max} \cos(\frac{an}{b}\omega t - n\theta_s) \tag{16}$$

The harmonic amplitude of rotor MMF is:

$$F_{\max} = B_{\max} \alpha_i \frac{g}{\mu_0} \tag{17}$$

where $B_{\max}$ is the amplitude of the flux density produced by the PM in the air-gap, and α_i is the polar arc coefficient, $\alpha_i \approx \alpha_p/\tau$. Assuming that the magnetic permeability of the PM is the same as that of air, ignoring the effect of saturation, magnetic leakage and cogging, then $B_{\max} = 2h_m B_r/(g+2h_m)$, where h_m is the thickness of the permanent magnet, B_r is the residual magnetic induction strength of the PM, and g is the effective air-gap length.

When the MMF of the rotor rotates synchronously with the main wave MMF (a, b) of the stator, the Fourier series whose MMF harmonics are decomposed into odd-numbered terms can be expressed as [21]:

$$f_k = 2B_r\alpha_i\frac{g}{\mu_0}\frac{2h_m}{2h_m+g}\sum_{\substack{k=1,3,5\cdots\\ n=kp_0}}^{\infty}\frac{\sin(k\pi\alpha_i)}{k\pi\alpha_i/2}\cos(\frac{an}{b}\omega t - n\theta_s) \tag{18}$$

If the main wave of stator MMF $\mu = a = 1$, $\nu = n = p_0 = 5$, according to (18), the rotor MMF has only odd harmonics of (1, 5), (3, 15), (5, 25), etc. In other words, the number of space-time harmonics of rotor MMF is (k, kp_0).

C. INFLUENCE OF THE STATOR AND ROTOR MMF ON ELECTROMAGNETIC TORQUE

Taking a 12-slot 10-pole unit motor as an example, the influence of stator and rotor MMF harmonics on electromagnetic torque of three-phase PMSM with FSCW is analyzed. According to the above research, it can be known that the three-phase composite stator MMF harmonics generated by the fundamental current component of three-phase current i_a, i_b, i_c are (1, 1), (1, 5), (1, 7), etc. The third harmonic current component in i_a, i_b, i_c does not produce three-phase composite stator MMF harmonics; the fifth harmonic current component in i_a, i_b, i_c produces three-phase composite stator MMF harmonics, which are (5, 1), (5, 5), (5, 7), etc. The harmonic analysis of three-phase composite stator MMF generated by other harmonic components of current is the same, not listed one by one. The harmonic of rotor MMF include (1, 5), (3, 15), (5, 25), (7, 35), etc. If the stator current is sinusoidal, that is, the current has only the fundamental current component, and the rotor magnetic field is also sinusoidal distribution, that is, the rotor MMF is only (1, 5), then the interaction between the two will only produce constant torque, and will not produce 6th, 12th, etc. ripple torque; if the stator current is sinusoidal, but the rotor magnetic field contains odd harmonics, ripple torque will be generated; if the rotor magnetic field is sinusoidal, but the stator current contains odd harmonics, ripple torque will also be generated. For this example, the stator MMF which affects the average torque of the motor is 5th (main wave), and the stator MMF that can produce ripple torque are harmonics of multiple times of 5, such as 25, 35, 55, etc.

V. COMPARISON OF PERFORMANCE BETWEEN SINE ROTOR MOTOR AND SINE + 3RD ROTOR MOTOR

A. SINE-SHAPED ROTOR AND SINE + 3RD SHAPED ROTOR

The air-gap magnetic field waveform distortion caused by the stator slot is distorted will have an adverse effect on the operation of the motor, such as cogging torque, torque ripple, etc. Many methods can be used to reduce this effect such as a skew pole, skew slot [22], unequal pole arc coefficient of the permanent magnet [23], changing permanent magnet shape [24], opening auxiliary slot, and unequal slot width. For the low-speed high-torque spoke type permanent magnet motor proposed in this article, the air-gap flux density waveform can be close to a sinusoidal by optimizing the shape of the rotor sheet, and the cogging torque and torque ripple can be reduced without changing the shape of the permanent magnet. Besides, rectangular permanent magnets are easy to process and reduce waste.

The analysis in Section IV shows that no matter whether the supply current contains odd-numbered harmonics such as 1, 3, 5, 7, etc., the three-phase symmetrical winding will not produce the stator MMF that is multiples of 3rd and 3rd, so the third harmonic of the rotor MMF (for the main wave) is introduced into the sinusoidally distributed rotor MMF, then the interaction of the rotor MMF and the stator MMF will not produce additional ripple torque. Fig. 7 (a) is the shape of the sine rotor, and Fig. 7 (b) is the shape of the proposed rotor. It can be seen that whether it is a sine rotor or the proposed rotor, the air-gap length along the periphery of the stator non-uniformity. For the sine rotor in Fig. 7 (a), there is the following relationship:

$$g(\theta) = g_{\max} - A\cos(\frac{\pi\theta}{w_r}) \tag{19}$$

for the sine + 3rd rotor in Fig. 7 (b):

$$g(\theta) = g_{\max} - \left[A\cos(\frac{\pi\theta}{w_r}) - a\cos(\frac{3\pi\theta}{w_r})\right] \tag{20}$$

where a is the amplitude of the third harmonic introduced.

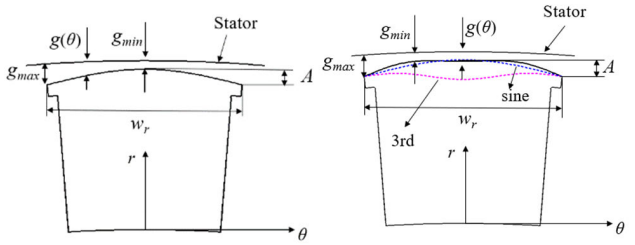

FIGURE 7. Rotor sheet shape. (a) Sine rotor (b) Sine + 3rd rotor.

If the width b_m and thickness h_m of the PM are kept unchanged, the maximum air-gap (g_{max}) and the minimum air-gap (g_{min}) are kept unchanged, the equivalent air-gap of the sine + 3rd rotor motor is smaller than that of the sine rotor motor, so the fundamental amplitude of rotor MMF is greater than that of sine rotor motor. Through the finite element analysis, the rotor MMF and the frequency spectrum when the armature current is 0 are obtained, as shown in Figs. 8 and 9.

Fig. 8 and Fig. 9 show that the main wave MMF (5th order) of the sine + 3rd rotor is larger than that of the sine rotor and, at the same time, a higher amplitude 15th MMF harmonic (relative to the main wave is 3th) is introduced in the air-gap. Due to the influence of core saturation and tooth tip leakage, both of them will produce other MMF harmonics

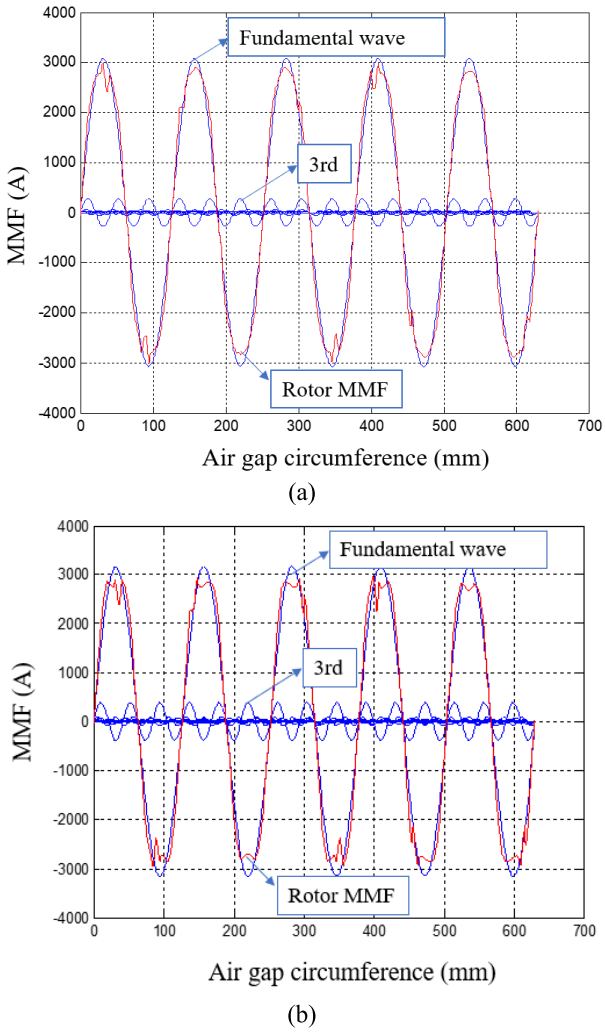

FIGURE 8. MMF of the rotor. (a) Sine rotor (b) Sine + 3rd rotor.

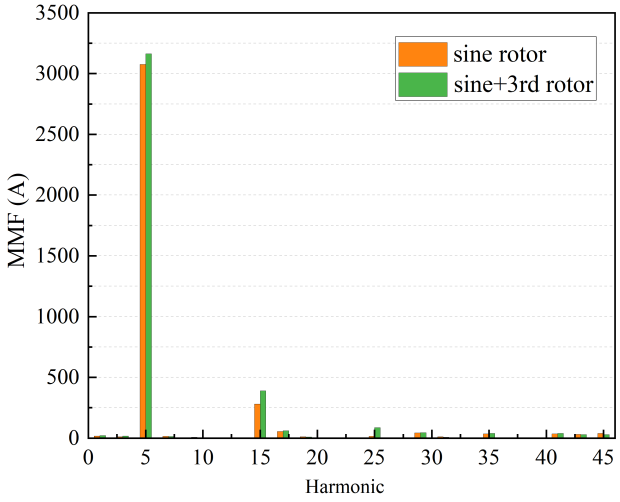

FIGURE 9. FFT of rotor MMF of sine rotor and Sine + 3rd rotor.

with lower amplitude. Theoretically, under the condition of sine wave current excitation and the same stator MMF, the average output torque of the proposed sine + 3rd rotor motor is larger than that of the sine rotor motor, the ripple torque will not increase. It should be noted that the MMF referred to in the simulation is the MMF generated by the permanent magnets. It does not fully participate in the torque generation, and there is a part of the leakage flux, which needs to be considered in the calculation.

B. FEA AND TORQUE PERFORMANCE COMPARISON

In order to verify the correctness of the optimization method proposed in this article, a spoke type permanent magnet direct drive motor for mine belt conveyors, as shown in Fig. 1, was designed, and electromagnetic field simulation analysis was performed to compare the electromagnetic performance of three different rotor shape motors. The main design parameters of the motor are shown in Table 1. Only the rotor shape of the three motors is different, and other parameters are the same. For the conventional rotor, $g_{max} = g_{min} = 2$mm. The finite element simulation results are shown in Figs. 10-14.

TABLE 1. Main parameter of the motor.

Parameter	Value
Rated power/kW	132
Rated phase voltage/V	620
Rated speed/rpm	60
Rated current/A	79
Number of poles/slots	40/48
Air-gap g_{max}/g_{min}/mm	4.0/2.0
Stator outer diameter/mm	950
Stator inner diameter/mm	760
Rotor outer diameter/mm	756
Rotor inner diameter/mm	676
Core length/mm	650
Conductors per slot	64
Parallel branches	2
Effective pole-arc coefficient	0.8272
Relative permeability	1.0605
Magnet remanence/T	1.23
Width of PM/mm	35
Thickness of PM/mm	14
Current density/A/mm^2	3.05

Fig. 10 shows the distribution of flux density cloud of sine + 3rd rotor motor, and the main magnetic circuit is not incredibly saturated. Fig. 11 (a) and (b) show the air-gap flux density and harmonic content. As shown in Fig. 11 (b), the fundamental amplitude of the air-gap flux density of the sine rotor motor is reduced compared with the conventional rotor motor. However, the sine + 3rd rotor can compensate for this decrease. Simultaneously, compared with the sine rotor motor, the air-gap flux density harmonics amplitude of the sine + 3rd rotor motor has not increased except for the third harmonic. Fig. 12 shows the no-load phase EMF waveform and harmonic content of motors with different rotor shapes. It can be seen that the effective value of back EMF of conventional rotor structure motor is the highest, and that of the sine rotor motor is the lowest, which is about 4.15%

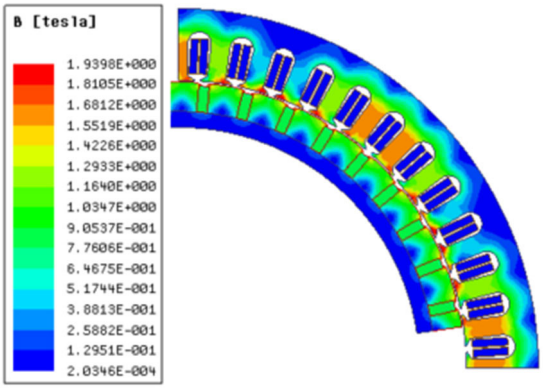

FIGURE 10. Flux density distribution of motor (sine + 3rd rotor).

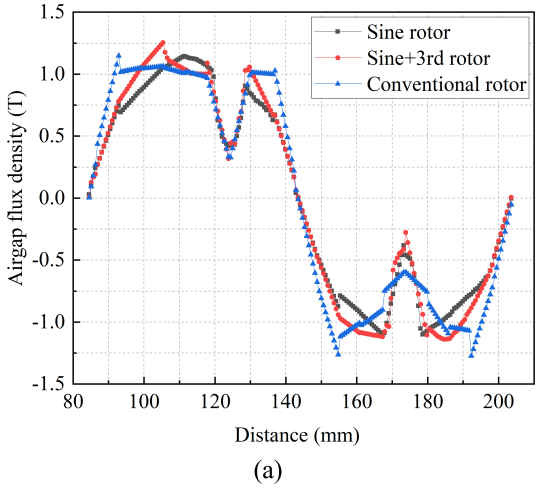

FIGURE 11. No-load air-gap flux density. (a) Waveforms (b) Harmonics.

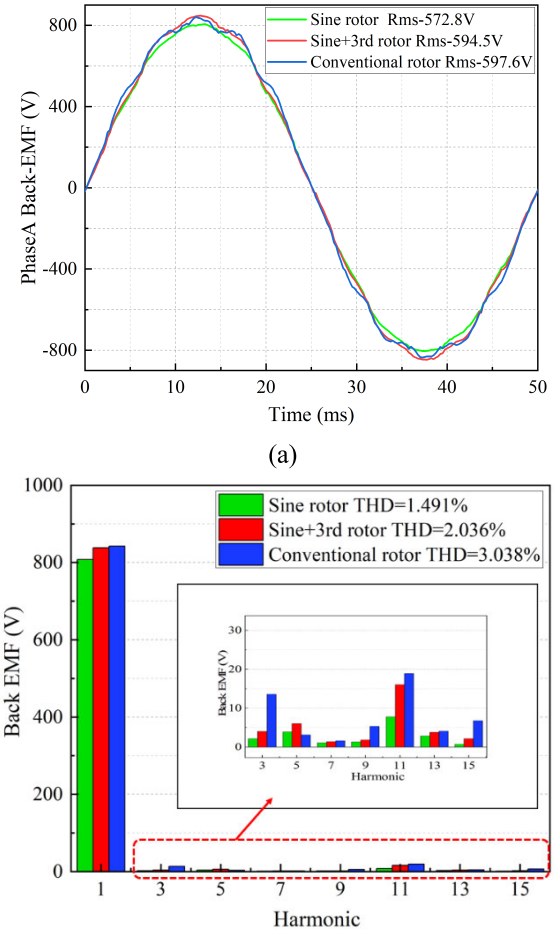

FIGURE 12. No-load Back-EMFs (60rpm). (a) Waveforms (b) Harmonics.

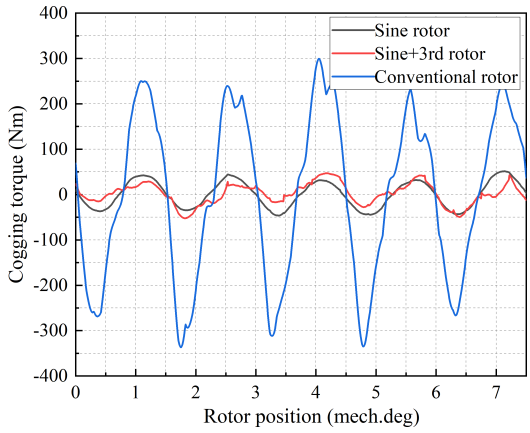

FIGURE 13. Comparison of cogging torque performance.

lower. However, by introducing the third harmonic into the sine-shaped rotor, the back EMF increases by 3.79%.

The cogging torque depends on the least common multiple between the number of slots and the number of poles [25]. Although the three motors all use the same stator, the peak-to-peak value of the cogging torque is different due to the influence of the rotor shape, as shown in Fig. 13. That is because different rotor shapes result in different air-gap flux density distribution and its harmonic content, as shown in Fig. 11 (a) and (b). It is also found that the peak-to-peak cogging torque of the conventional rotor spoke type motor and the sine-shaped rotor motor is the highest and

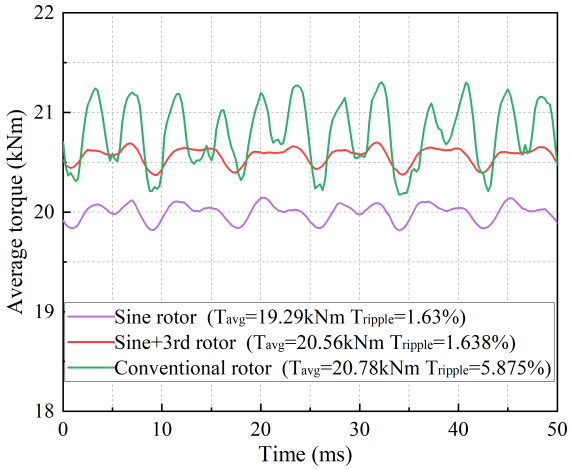

FIGURE 14. Comparison of average torque performance.

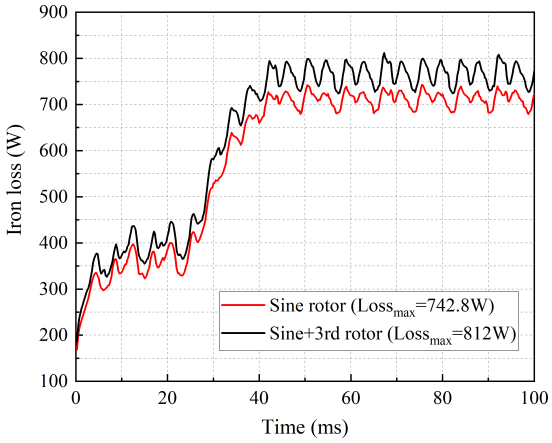

FIGURE 15. The loss of stator iron.

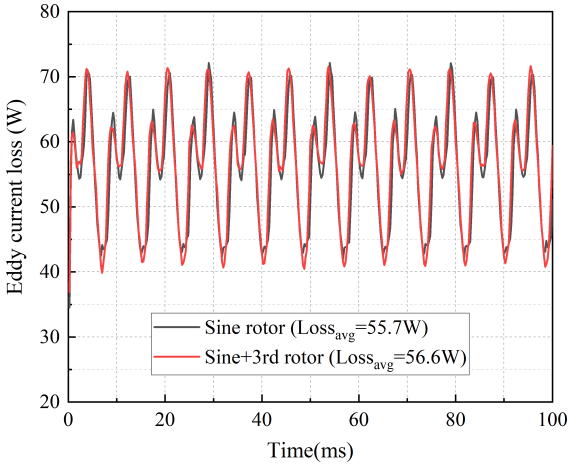

FIGURE 16. The eddy current loss of PM.

the lowest, respectively. Compared with the sine rotor motor, the cogging torque of the sine + 3rd rotor motor is slightly increased. Fig. 14 shows the rated output torque performance of motors with different rotor shapes under the sinusoidal current excitation. The torque ripple is further calculated by the following formula, which is the ratio of the peak-to-peak torque to the average torque [24]:

$$T_{ripple} = \frac{T_{\max} - T_{\min}}{T_{avg}} \cdot 100\% \tag{21}$$

The results show that the average torque of conventional rotor motor is the highest, while that of sine rotor motor is the smallest. Compared with the sine rotor motor, the average torque of the sine + 3rd rotor motor is increased by more than 6.58%, and the simulation results are consistent with the previous theoretical analysis. That is because of the variation of the equivalent air-gap length caused by different rotor sheet shapes, as shown in Fig. 7 (a) and (b). Simultaneously, the torque ripple of the sine + 3rd rotor and sine rotor motor is very similar, but they are far lower than the conventional rotor motor. That is because the low order harmonics in the back EMF of sine rotor and sine + 3rd rotor motors are significantly reduced (as shown in Fig. 12(b)), which will interact with the armature current to produce 6th and 12th harmonic torques. Theoretically, there is no ripple torque in the sine rotor motor under the sinusoidal power supply, which is caused by core saturation and tooth tip flux leakage, mainly the 6th and 12th ripple torque. After introducing the third harmonic, the main wave amplitude of rotor MMF will be increased, and the harmonic amplitude of the rotor MMF will also be affected, thus affecting the ripple torque and cogging torque. But most importantly, the proposed rotor structure improves the average torque based on a small increase in cogging torque and torque ripple.

C. COMPARISON OF LOSS

The analysis in the previous section shows that for a spoke type permanent magnet direct drive motor, and the average torque can be improved without increasing cogging torque and torque ripple after introducing the third rotor MMF harmonic into the sine rotor sheet. However, it should be noted that while the sine + 3rd rotor increases the fundamental wave amplitude of the rotor MMF, it also increases the third harmonic amplitude, as shown in Figs. 8-9. The other harmonics may cause undesirable effects, such as localized saturation, additional iron loss, and eddy current loss in the magnets, etc. [26].

In this section, the stator iron loss and PM eddy current loss of sine rotor motor and sine + 3rd rotor motor are compared. The loss under rated load is calculated by FEM, as shown in Figs. 15-16. It is easy to find that the stator iron loss of the sine + 3rd rotor motor is slightly greater than that of the sine rotor motor, and the eddy current loss of the PM is basically unchanged, which indicates that the introduction of the third rotor MMF harmonic does not affect the loss of the prototype. This is because the prototype proposed in this article is a low-speed high-torque permanent magnet motor with a low rated frequency of only 20Hz. Therefore, the introduction of rotor MMF harmonic has little effect on the iron loss of the motor. Moreover, the permanent magnet is embedded, eddy current reaction mainly occurs on the surface of the rotor, and

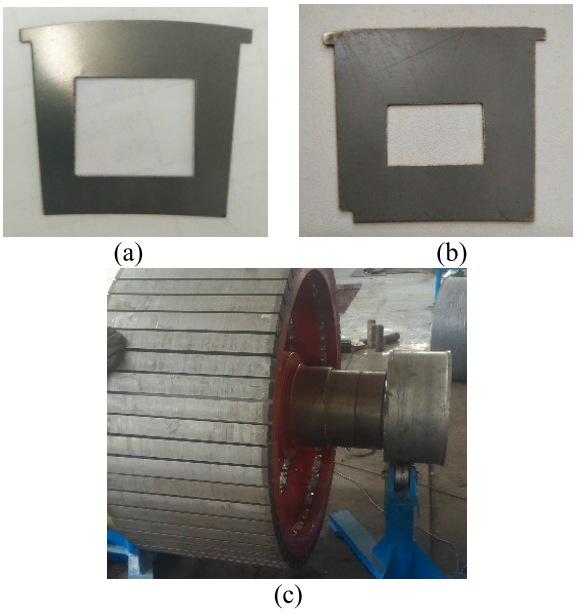

FIGURE 17. Rotor sheet shape. (a) Sine rotor (b) Sine + 3rd rotor (c) Rotor complete.

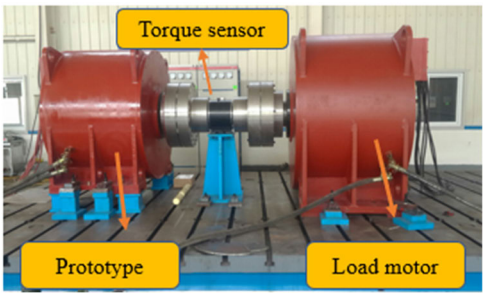

FIGURE 18. Prototype experimental platform.

skin effect is not obvious, so there is basically no change in the eddy current loss of the PM. However, for the high-speed PM motor with high rated frequency, the proposed torque optimization method may increase the iron loss and eddy current loss of the PM, which will lead to severe heating and low efficiency of the motor, which is worth noting.

D. EXPERIMENT AND PROTOTYPE

To verify the correctness and effectiveness of the optimization method proposed in this article, we produce two spoke type permanent magnet direct-drive motors: sine rotor and sine + 3rd rotor. Fig. 17. shows the appearance of a single rotor sheet. Fig. 18 shows the motor loading experiment platform. A 250kW permanent magnet direct drive motor is used as the load motor to measure the torque characteristics of the prototype. The torque sensor is equipped with a digital display and measures the output torque and speed. In the experiment, the direct torque control mode is used to control the load motor, and the speed is set to 0 rpm, the load motor is in the state of power generation; the sensorless vector control mode is used to control the prototype, and the tested motor is in

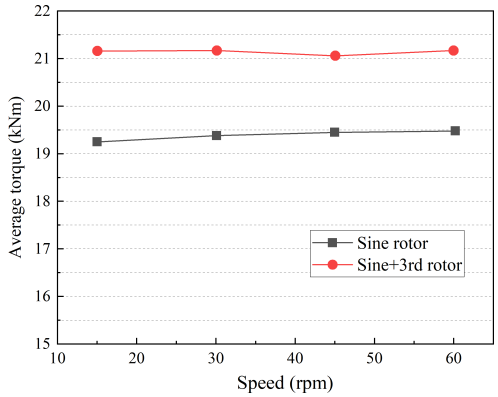

FIGURE 19. Torque-speed curves.

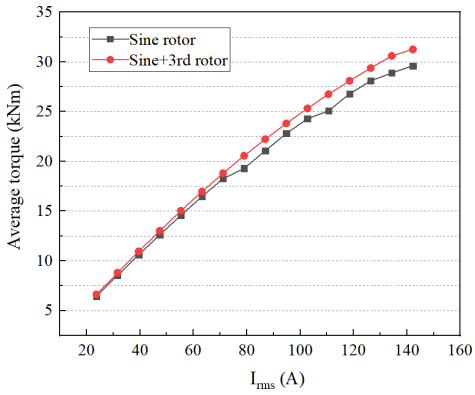

FIGURE 20. The curves of average torque versus current (60rpm).

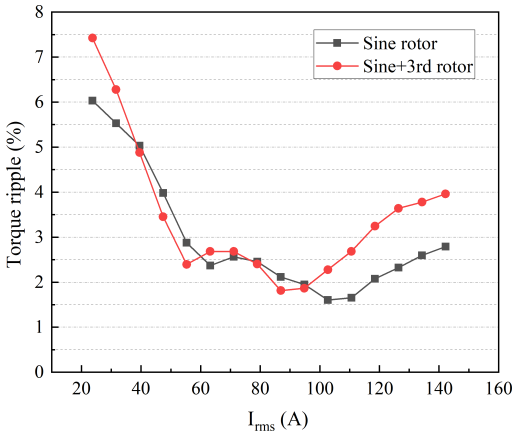

FIGURE 21. Variation of torque ripple with load current (60rpm).

the electric state, and the speed is adjustable. Because of the limited experimental conditions, no experimental equipment can measure the torque waveform in real-time. We record the maximum and minimum torques obtained by the digital display at a particular current or a certain speed and then perform data processing to obtain the average torque curve and torque ripple curve.

Fig. 19 shows the experimental results of full load speed regulation. Fig. 20 shows the relationship curve between average torque and current, and Fig. 21 shows the variation

of torque ripple with load current. The results show that the proposed motor has good low-speed and high-torque characteristics and can achieve constant torque operation within the rated speed, which is very suitable for direct-drive applications such as belt conveyor load. Compared with the sine rotor motor, the output average torque of the optimized motor has been increased by about 8.5%, and the variation trend of torque ripple is the same. The torque ripple is very close to the same near the rated point of the motor, but it is larger than the finite element analysis results. The reason is that the power supply is the PWM wave, and the current contains a harmonic component. Through experiments, it is also found that when the armature current $I < 1.2IN$, the torque and current are approximately linearly related. With the further increase of current I, the speed of torque increase begins to decrease. This is because with the increase of armature current, the armature reaction of the motor is enhanced, and the saturation degree of the magnetic circuit of the motor increases. The relationship between the output torque and the current of the motor presents a certain nonlinear, and the torque ripple also begins to increase simultaneously.

VI. CONCLUSION

This article presents a torque optimization method of rotor shape by introducing the third rotor MMF harmonics, which can improve the average torque of the motor when the cogging torque and torque ripple increases little. It is suitable for driving systems such as mine belt conveyors that require high torque density and low torque ripple of permanent magnet direct drive motors. Through theoretical analysis, it reveals that the stator and rotor MMF harmonic interactions with the same space order and the same time order consistent with the main wave speed produce a constant electromagnetic torque; pulsating electromagnetic torque is generated by the interaction of stator and rotor MMF with the same order and space order inconsistent with the main wave speed; otherwise, no torque will be generated. It provides a theoretical basis for improving torque density and reducing torque ripple. The influence of stator and rotor MMF harmonics on electromagnetic torque of three-phase FSCW spoke type structure PMSM is analyzed by the analytical method. The torque performance and loss of the motor before and after optimization are compared and analyzed under the sine wave power supply using the finite element software. The prototype experiment is carried out to verify the correctness and effectiveness of the optimization method proposed in this article.

REFERENCES

[1] A. M. El-Refaie, "Fractional-slot concentrated-windings synchronous permanent magnet machines: Opportunities and challenges," *IEEE Trans. Ind. Electron.*, vol. 57, no. 1, pp. 107–121, Jan. 2010.

[2] B. Kim and T. A. Lipo, "Design of a surface PM Vernier motor for a practical variable speed application," in *Proc. IEEE Energy Convers. Congr. Expo. (ECCE)*, Montreal, QC, Canada, Sep. 2015, pp. 776–783.

[3] P. B. Reddy, A. M. El-Refaie, and K.-K. Huh, "Effect of number of layers on performance of fractional-slot concentrated-windings interior permanent magnet machines," *IEEE Trans. Power Electron.*, vol. 30, no. 4, pp. 2205–2218, Apr. 2015.

[4] M. Onsal, B. Cumhur, Y. Demir, E. Yolacan, and M. Aydin, "Rotor design optimization of a new flux-assisted consequent pole spoke-type permanent magnet torque motor for low-speed applications," *IEEE Trans. Magn.*, vol. 54, no. 11, pp. 1–5, Nov. 2018.

[5] K.-Y. Hwang, S.-B. Rhee, J.-S. Lee, and B.-I. Kwon, "Shape optimization of rotor pole in spoke type permanent magnet motor for reducing partial demagnetization effect and cogging torque," in *Proc. Int. Conf. Electr. Mach. Syst. (ICEMS)*, Seoul, South Korea, 2007, pp. 955–960.

[6] M. Barcaro, N. Bianchi, and F. Magnussen, "Six-phase supply feasibility using a PM fractional-slot dual winding machine," *IEEE Trans. Ind. Appl.*, vol. 47, no. 5, pp. 2042–2050, Sep./Oct. 2011.

[7] W. Zhao, J. Zheng, J. Ji, S. Zhu, and M. Kang, "Star and delta hybrid connection of a FSCW PM machine for low space harmonics," *IEEE Trans. Ind. Electron.*, vol. 65, no. 12, pp. 9266–9279, Dec. 2018.

[8] C. Yiguang, "Inductance calculation of permanent magnet synchronous machines with fractional-slot concentrated winding," *Trans. China Electrotech. Soc.*, vol. 29, pp. 119–124, Jan. 2014.

[9] A. M. El-Refaie and T. M. Jahns, "Optimal flux weakening in surface PM machines using fractional-slot concentrated windings," *IEEE Trans. Ind. Appl.*, vol. 41, no. 3, pp. 790–800, May/Jun. 2005.

[10] Y. Li, J. Xing, T. Wang, and Y. Lu, "Programmable design of magnet shape for permanent-magnet synchronous motors with sinusoidal back EMF waveforms," *IEEE Trans. Magn.*, vol. 44, no. 9, pp. 2163–2167, Sep. 2008.

[11] P. Zheng, J. Zhao, J. Han, J. Wang, Z. Yao, and R. Liu, "Optimization of the magnetic pole shape of a permanent-magnet synchronous motor," *IEEE Trans. Magn.*, vol. 43, no. 6, pp. 2531–2533, Jun. 2007.

[12] N. Roshandel Tavana and A. Shoulaie, "Analysis and design of magnetic pole shape in linear permanent-magnet machine," *IEEE Trans. Magn.*, vol. 46, no. 4, pp. 1000–1006, Apr. 2010.

[13] Z. S. Du and T. A. Lipo, "High torque density and low torque ripple shaped-magnet machines using sinusoidal plus third harmonic shaped magnets," *IEEE Trans. Ind. Appl.*, vol. 55, no. 3, pp. 2601–2610, May/Jun. 2019.

[14] D. Wang, X. Wang, and S.-Y. Jung, "Cogging torque minimization and torque ripple suppression in surface-mounted permanent magnet synchronous machines using different magnet widths," *IEEE Trans. Magn.*, vol. 49, no. 5, pp. 2295–2298, May 2013.

[15] D. Wu and Z. Q. Zhu, "Design tradeoff between cogging torque and torque ripple in fractional slot surface-mounted permanent magnet machines," *IEEE Trans. Magn.*, vol. 51, no. 11, pp. 1–4, Nov. 2015.

[16] Z. Zhang, S. Yu, F. Zhang, S. Jin, and X. Wang, "Electromagnetic and structural design of a novel low-speed high-torque motor with dual-stator and PM-reluctance rotor," *IEEE Trans. Appl. Supercond.*, vol. 30, no. 4, pp. 1–5, Jun. 2020.

[17] F. Zhao, T. A. Lipo, and B.-I. Kwon, "A novel dual-stator axial-flux spoke-type permanent magnet Vernier machine for direct-drive applications," *IEEE Trans. Magn.*, vol. 50, no. 11, pp. 1–4, Nov. 2014.

[18] Y. Zhu, H. Wu, and J. Zhang, "Regenerative braking control strategy for electric vehicles based on optimization of switched reluctance generator drive system," *IEEE Access*, vol. 8, pp. 76671–76682, 2020.

[19] Y. Zhu, W. Wei, C. Yang, and Y. Zhang, "Multi-objective optimisation design of two-phase excitation switched reluctance motor for electric vehicles," *IET Electr. Power Appl.*, vol. 12, no. 7, pp. 929–937, Aug. 2018.

[20] S. Xu, *Windings Theory of AC Machines*, 1st ed. Beijing, China: China Machine Press, 1985, pp. 107–119.

[21] A. B. Proca, A. Keyhani, A. EL-Antably, W. Lu, and M. Dai, "Analytical model for permanent magnet motors with surface mounted magnets," *IEEE Trans. Energy Convers.*, vol. 18, no. 3, pp. 386–391, Sep. 2003.

[22] C. Xia, Z. Zhang, and Q. Geng, "Analytical modeling and analysis of surface mounted permanent magnet machines with skewed slots," *IEEE Trans. Magn.*, vol. 51, no. 5, pp. 1–8, May 2015.

[23] B. Peng, W. Zhao, and X. Wang, "The method for reducing intrinsic shaft voltage by suitable selection of pole-arc coefficient in fractional-slot permanent-magnet synchronous machines," *IEEE Trans. Magn.*, vol. 54, no. 11, pp. 1–5, Nov. 2018.

[24] Y.-P. Yang and M.-T. Peng, "A surface-mounted permanent-magnet motor with sinusoidal pulsewidth-modulation-shaped magnets," *IEEE Trans. Magn.*, vol. 55, no. 1, pp. 1–8, Jan. 2019.

[25] Z. Q. Zhu and D. Howe, "Influence of design parameters on cogging torque in permanent magnet machines," *IEEE Trans. Energy Convers.*, vol. 15, no. 4, pp. 407–412, Dec. 2000.
[26] F. Magnussen and H. Lendenmann, "Parasitic effects in PM machines with concentrated windings," *IEEE Trans. Ind. Appl.*, vol. 43, no. 5, pp. 1223–1232, Sep./Oct. 2007.

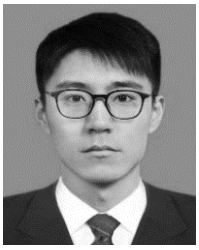

JIAXU ZHANG received the B.S. degree in electrical engineering and automation from the Shenyang University of Technology, Shenyang, China, in 2016, where he is currently pursuing the Ph.D. degree in electrical engineering. His research interest includes design and control of permanent magnet motor.

BINGYI ZHANG received the B.S., M.S., and Ph.D. degrees in electrical engineering from the Shenyang University of Technology, Shenyang, China, in 1982, 1987, and 2007, respectively. He is currently a Professor with the Shenyang University of Technology. His research interests include design and optimization of electrical machines, low-speed high-torque drive systems, and power system automation.

GUIHONG FENG received the B.S. degree in electrical engineering from the Shenyang University of Technology, Shenyang, China, in 1985, and the M.S. degree in electric drive and automation from Northeastern University, Shenyang, in 1994. She is currently a Professor with the Shenyang University of Technology. Her research interests include design and optimization of electrical machines, low-speed high-torque drive systems, and power system automation.